Hybrid polarizing solids for pure hyperpolarized liquids through dissolution dynamic nuclear polarization

David Gajan[a], Aurélien Bornet[b], Basile Vuichoud[b], Jonas Milani[b], Roberto Melzi[c], Henri A. van Kalkeren[d], Laurent Veyre[d], Chloé Thieuleux[d], Matthew P. Conley[e], Wolfram R. Grüning[e], Martin Schwarzwälder[e], Anne Lesage[a], Christophe Copéret[e], Geoffrey Bodenhausen[b,f,g,h], Lyndon Emsley[a,b,1], and Sami Jannin[b]

[a]Centre de Résonance Magnétique Nucléaire (RMN) à Très Hauts Champs, Institut des Sciences Analytiques [Centre National de la Recherche Scientifique (CNRS)/Ecole Normale Supérieure (ENS) Lyon/Université Claude Bernard Lyon 1 (UCBL)], Université de Lyon, 69100 Villeurbanne, France; [b]Institut des Sciences et Ingénierie Chimiques, Ecole Polytechnique Fédérale de Lausanne (EPFL), CH-1015 Lausanne, Switzerland; [c]Bruker Italia S.r.l., IT-20158 Milan, Italy; [d]Université de Lyon, Institut de Chimie de Lyon, Laboratoire de Chimie, Catalyse, Polymères et Procédés (LC2P2), Unité Mixte de Recherche (UMR) 5265 Centre National de la Recherche Scientifique (CNRS)-Ecole Supérieure de Chimie Physique Electronique de Lyon (CPE Lyon)-Université Claude Bernard Lyon 1 (UCBL), Ecole Supérieure de Chimie Physique Electronique de Lyon (CPE Lyon), 69100 Villeurbanne, France; [e]Department of Chemistry and Applied Biosciences, Eidgenössiche Technische Hochschule (ETH), 8093 Zurich, Switzerland; [f]Département de Chimie, Ecole Normale Supérieure (ENS)-Paris Sciences et Lettres (PSL) Research University, F-75005 Paris, France; [g]Laboratoire de Biomolécules (LBM), Université Pierre et Marie Curie (UPMC) Université Paris 06, Sorbonnes Universités, F-75005 Paris, France; and [h]Laboratoire de Biomolécules (LBM), Unité Mixte de Recherche (UMR) 7203 Centre National de la Recherche Scientifique (CNRS), F-75005 Paris, France

Edited* by Timothy M. Swager, Massachusetts Institute of Technology, Cambridge, MA, and approved August 25, 2014 (received for review April 30, 2014)

Hyperpolarization of substrates for magnetic resonance spectroscopy (MRS) and imaging (MRI) by dissolution dynamic nuclear polarization (D-DNP) usually involves saturating the ESR transitions of polarizing agents (PAs; e.g., persistent radicals embedded in frozen glassy matrices). This approach has shown enormous potential to achieve greatly enhanced nuclear spin polarization, but the presence of PAs and/or glassing agents in the sample after dissolution can raise concerns for in vivo MRI applications, such as perturbing molecular interactions, and may induce the erosion of hyperpolarization in spectroscopy and MRI. We show that D-DNP can be performed efficiently with hybrid polarizing solids (HYPSOs) with 2,2,6,6-tetramethyl-piperidine-1-oxyl radicals incorporated in a mesostructured silica material and homogeneously distributed along its pore channels. The powder is wetted with a solution containing molecules of interest (for example, metabolites for MRS or MRI) to fill the pore channels (incipient wetness impregnation), and DNP is performed at low temperatures in a very efficient manner. This approach allows high polarization without the need for glass-forming agents and is applicable to a broad range of substrates, including peptides and metabolites. During dissolution, HYPSO is physically retained by simple filtration in the cryostat of the DNP polarizer, and a pure hyperpolarized solution is collected within a few seconds. The resulting solution contains the pure substrate, is free from any paramagnetic or other pollutants, and is ready for in vivo infusion.

D-DNP | NMR signal enhancement | molecular imaging | mesostructured hybrid silica | porous materials

Dissolution dynamic nuclear polarization (D-DNP) (1, 2) usually requires freezing molecules of interest, such as metabolites, together with persistent free radicals often called polarizing agents (PA) in a glassy matrix at very low temperatures ($1 < T < 4$ K), so that their nuclear spin polarization can be enhanced by up to four to five orders of magnitude. Such enhancements are achieved by saturating the ESR transitions of the PAs. D-DNP is generally performed in moderate magnetic fields ($B_0 = 3.35$ or in this study, 6.7 T) and followed by rapid dissolution of the frozen sample with a burst of superheated water to give highly polarized solutions. Applications include detection of intermediates in chemical reactions (3–5), protein folding in real time (6), and detection of cancer by monitoring abnormal rates of metabolic reactions in humans (7). PAs with narrow EPR lines, such as trityl radicals, are usually used for the direct polarization of ^{13}C nuclei (2). In practice, polarizations $P(^{13}C)$ of 20% or higher can be obtained after dissolution. We have recently shown that DNP of ^{13}C can be significantly accelerated by combining increased magnetic fields with polarization of ^{1}H rather than ^{13}C [using nitroxide radicals, such as 2,2,6,6-tetramethyl-piperidine-1-oxyl (TEMPO), with broader ESR lines than trityl radicals] followed by Hartmann–Hahn $^{1}H \rightarrow {}^{13}C$ cross-polarization (CP) (8) to transfer the polarization from ^{1}H to ^{13}C. In this way, $P(^{13}C) = 40\%$ after dissolution at 300 K was obtained in less than 20 min (9–13).

Longitudinal relaxation during heating, dissolution, transfer between magnets, and magnetic resonance spectroscopy or MRI measurements themselves erodes hyperpolarization. Relaxation losses are exacerbated by remaining paramagnetic PAs that no longer serve any function after dissolution; thus, one of the most effective ways to slow down the relaxation rate $R_1(^{13}C)$ and hence, prolong the lifetime of the polarization $P(^{13}C)$ is to eliminate the radicals (14). For some radicals, such as trityls, separation can be achieved by solvent extraction (15) or precipitation by a jump in pH followed by mechanical filtration through a stack of polyethylene filters (16, 17). Lumata et al. (18, 19) have shown that precipitation can be used for 1,3 bisdiphenylene-2-phenylallyl (BDPA) and 2,2 diphenyl-1-picrylhydrazyl (DPPH). For TEMPO, with its derivatives including most currently used biradicals (20–26), we have

Significance

Hyperpolarization by dissolution dynamic nuclear polarization can dramatically enhance signal intensities in MRI and NMR, notably for metabolic tracers for imaging and diagnosis. It is applicable to a variety of substrates for in vivo imaging and chemistry but requires the use of contaminants (glassing agents and free radicals) that may interact with cells and proteins and can have potential side effects. These contaminants can sometimes be eliminated by precipitation followed by filtration or solvent extraction, but these methods are substrate-specific, are usually time-consuming, and typically result in signal loss. Here, production of pure hyperpolarized liquids free of contaminants is shown by a simple wetting–polarization–filtration sequence for a solid silica matrix containing homogeneously distributed persistent radicals.

Author contributions: D.G., A.L., C.C., G.B., L.E., and S.J. designed research; D.G., A.B., B.V., J.M., H.A.v.K., L.V., M.P.C., W.R.G., M.S., and S.J. performed research; H.A.v.K., M.P.C., W.R.G., and M.S. contributed new reagents/analytic tools; D.G., A.B., B.V., J.M., R.M., C.T., A.L., C.C., G.B., L.E., and S.J. analyzed data; and D.G., C.T., C.C., G.B., L.E., and S.J. wrote the paper.

The authors declare no conflict of interest.

*This Direct Submission article had a prearranged editor.

Freely available online through the PNAS open access option.

[1]To whom correspondence should be addressed. Email: lyndon.emsley@ens-lyon.fr.

This article contains supporting information online at www.pnas.org/lookup/suppl/doi:10.1073/pnas.1407730111/-/DCSupplemental.

shown that chemical PA quenching with sodium ascorbate (vitamin C) can convert the nitroxide radicals into diamagnetic species through reduction (14). However, for quantitative and rapid quenching, ascorbate must be used in excess, and the remaining ascorbate in solution may affect the analyte or sensitive components present in the NMR or MRI system, such as enzymes (5, 27, 28). Furthermore, the presence of potentially noninnocent additional products arising from the paramagnetic PAs is obviously undesirable for in vivo MRI experiments. In this light, methods to produce pure hyperpolarized solutions free of radicals, glassing, and reducing agents with a limited number of production steps could enable faster, safer, and more sensitive in vitro and in vivo applications.

Eichhorn et al. (29) have recently proposed a promising method for producing hyperpolarized pyruvate solutions without

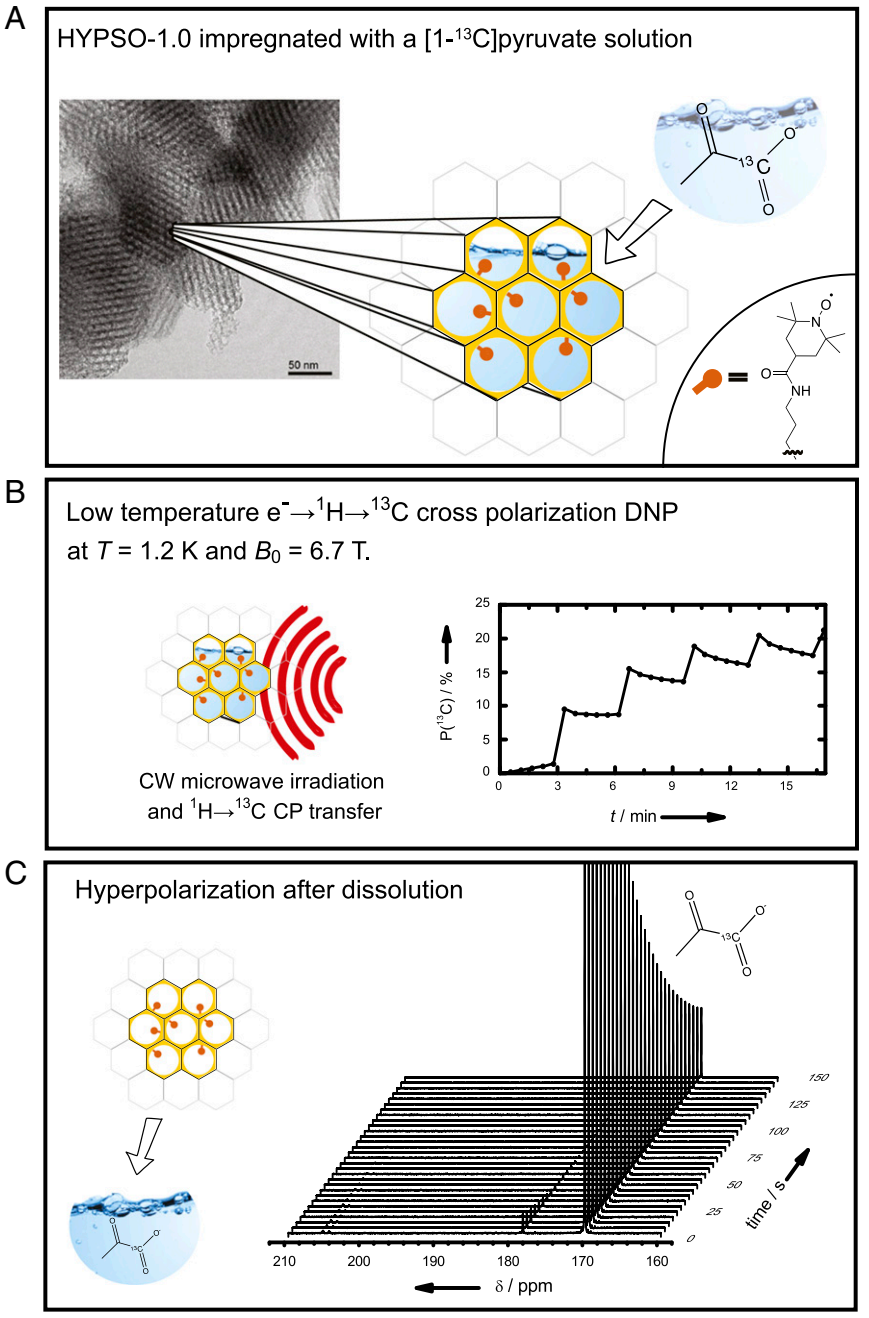

Fig. 1. Hyperpolarization by D-DNP with HYPSO. (*A*) HYPSO 1.0 is impregnated with a solution of the analyte to be polarized without addition of any glass-forming agents. The transmission EM image (taken with a Philips CM30 TEM operated at 300 kV) shows the porous structure of the material. The red dots schematically represent the PAs. (*B*) Proton DNP is performed (*Methods*) on 20 mg HYPSO 1.0 material (88 μmol/g) impregnated with 36 μL 3 M solution of [1-^{13}C]-pyruvate in D_2O. The proton polarization rapidly builds up with a time constant $\tau_{DNP}(^1H) = 119 \pm 1.5$ s, and by applying $^1H \rightarrow ^{13}C$ CP, a polarization of $P(^{13}C) > 20\%$ is reached in 17 min. CW, continuous wave. (*C*) The DNP solution is dissolved and expulsed from HYPSO 1.0 by injecting 5 mL superheated D_2O (more details in *Methods*) and transferring to a 300-MHz spectrometer; a series of ^{13}C NMR spectra of [1-^{13}C]-pyruvate is measured every 5 s. The liquid-state polarization obtained $P(^{13}C) = 25.3\%$ corresponds to an enhancement $\varepsilon_{DNP} > 32{,}000$ compared with the Boltzmann equilibrium at 300 K and 7 T, and decays with $T_1(^{13}C) = 49.4 \pm 0.4$ s are typical of a pure D_2O solution of [1-^{13}C]-pyruvate without any free radicals.

free radicals. This route consists in performing D-DNP on pure [1-^{13}C]-pyruvic acid, in which photo-induced radicals have been generated by intense UV radiation. However, the scope of D-DNP is certainly not limited to pyruvate but should encompass a wide variety of substrates that can be used as metabolic tracers, protein ligands, or chemical reagents. In fact, the UV irradiation process degrades some of the pyruvate into [1-^{13}C]-acetate, which may interfere in vivo, because it is also a metabolite in the Krebs cycle.

One approach to obtain highly polarized solutions free of radicals would be to use a solid polarizing matrix, which would be easily separable from the solution by filtration. Immobilization of radicals on solid materials, such as silica gels or thermoresponsive polymers (30–32), has been reported for room temperature Overhauser DNP of liquid water. More recently, low temperature DNP at $T = 4.2$ K was shown by exploiting electron spins at dangling bond sites near the surface of silicon nanoparticles, producing, however, only modest enhancements (~2) (33). One critical problem in solid polarizing matrices is to avoid polarization loss through radical–radical interactions; an optimal polarization matrix, thus, requires control of both the radical density and distribution in the solid.

Here, we show the high polarizing efficiency at very low temperatures (1.2 and 4.2 K) of hybrid polarizing solids (HYPSOs), a family of hybrid organosilica materials, prepared by a Sol-Gel process using a templating route, in which PAs are covalently linked to the pore channels and homogeneously randomly distributed in the mesostructured silica matrix (34). Such control of distribution is not accessible through classical grafting postfunctionalization approaches (34, 35). We show that, after polarization, radical-free hyperpolarized solutions can be easily and rapidly (<11 s) obtained by physical retention during dissolution. This approach leads to large ^{13}C polarization in the solid state, and we show that as much as $P(^{13}C) = 25.3\%$ is obtained in the liquid state after dissolution, corresponding to an enhancement factor $\varepsilon_{DNP} > 32{,}000$ with respect to the Boltzmann distribution at 7 T and 300 K. The whole approach is illustrated in Fig. 1.

Results and Discussion

The HYPSO family of mesostructured hybrid organosilica materials was chosen, because enhancement factors of up to $\varepsilon_{on/off} = 36$ were reported (34) under magic angle spinning-DNP (MAS-DNP) conditions at $T = 100$ K and $B_0 = 9.4$ T when impregnated with a water or 1,1,2,2-tetrachloroethane solution. The first generation of material, HYPSO 1.0, contains homogeneously distributed TEMPO moieties covalently bound to the silica surface through a propylamide linker [$O_{1.5}Si$–$(CH_2)_3$–NHCO–TEMPO] with varying radical concentration. HYPSO 1.0 has a large pore volume, which allows the polarization of up to ~1.8 mL solution per 1 g material through a complete filling of the pores (~1.0 mL/g) and the intergrain volumes (~0.8 mL/g). The effective filling factor amounts to $\eta = V_{solution}/V_{total} = 0.85$ (illustrating that the use of such materials does not significantly reduce the volume of polarized solution through the addition of the solid PA). After HYPSO 1.0 is impregnated with a solution of interest, routine DNP can readily be performed in a standard manner by microwave irradiation of the ESR transition. In addition, the covalent linkage between the PA and the silica matrix allows the PAs to remain attached to the surface of the solid matrix during the combined dissolution and filtration step to produce a pure hyperpolarized solution (vide infra). The solution is easily expelled from HYPSO 1.0 by injecting hot water under pressure ($T_{diss} = 450$ K, $P_{diss} = 1$ MPa), which is usually done for regular frozen glassy DNP samples. The resulting slurry is then forced by pressurized hot water with a helium pressure of $P_{push} = 6$ MPa through a home-built cellulose fiber filter mounted just above the DNP sample holder as near as possible to the center of the 6.7-T magnetic field of the polarizer.

Data in Fig. 1 were recorded with 20 mg HYPSO 1.0 material containing 88 μmol radical per gram (the optimal concentration to obtain the highest polarization and the best buildup rate; see below) impregnated with 36 μL 3 M solution of [1-^{13}C]-pyruvate in D_2O. After impregnation (Fig. 1*A*), the sample is inserted into our home-built DNP polarizer operating at 6.7 T (11, 12, 36–38); 20 min of polarization (more details in *Methods*) suffice for $P(^{13}C)$ to exceed 20% (Fig. 1*B*). The monoexponential DNP buildup (absence of long-range spin diffusion behavior) confirms that the solution has filled the pores of the material. Dissolution is subsequently performed by injecting 5 mL superheated water (working equally well with D_2O or H_2O) at $T = 450$ K and $P = 1$ MPa. During this process, the entire hyperpolarized solution is expelled from the pores of the material (as determined by quantitative ^{1}H NMR), whereas the PAs remain attached to the surface of the solid. The solution is then transferred to a 7-T NMR spectrometer (300 MHz for protons), and the hyperpolarized [1-^{13}C]-pyruvate signal is measured with an enhancement factor $\varepsilon_{DNP} = 32{,}500$ compared with its thermal equilibrium signal after complete relaxation corresponding to a polarization $P(^{13}C) = 25.3\%$ (Fig. 1*C*). Note that the entire process—dissolution, separation, and polarization measurement at room temperature—requires only 10.2 s, clearly showing the efficiency of this

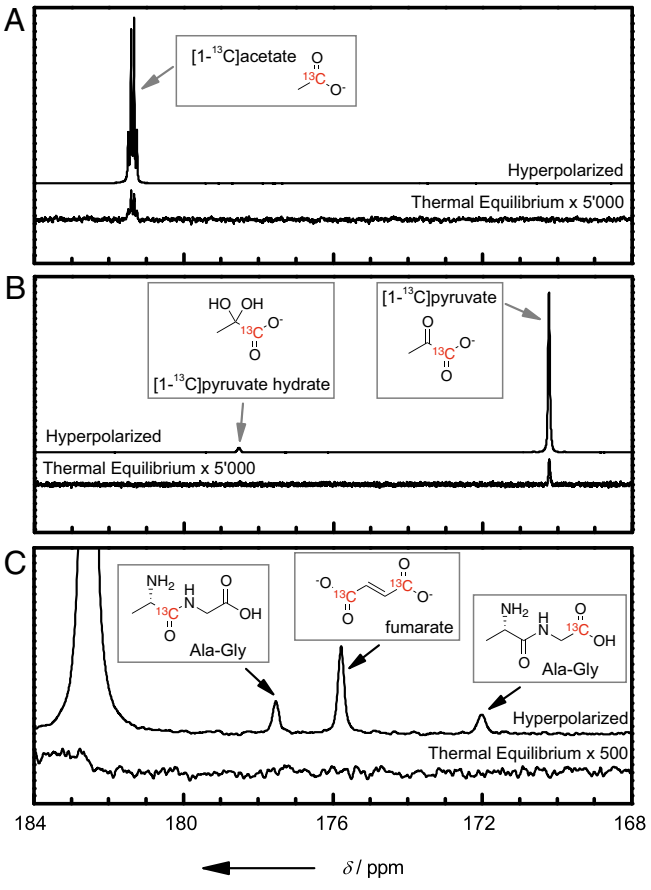

Fig. 2. Hyperpolarized [1-^{13}C]-acetate, [1-^{13}C]-pyruvate, L-alanine-glycine, and fumarate. Thermal equilibrium and hyperpolarized signals of (*A*) [1-^{13}C]-acetate, (*B*) [1-^{13}C]-pyruvate, and (*C*) L-alanine-glycine and fumarate. Hyperpolarization was performed as described in the text by ^{1}H→^{13}C CP-DNP with HYPSO 1.0 followed by dissolution. The hyperpolarized signals were acquired with single 5° nutation angle pulses, whereas the thermal equilibrium signals, scaled by a factor of 5,000, were measured with 27, 128, and 512 scans for [1-^{13}C]-acetate, [1-^{13}C]-pyruvate, and L-alanine-glycine and fumarate, respectively, using 90° nutation angle pulses applied every 300 s.

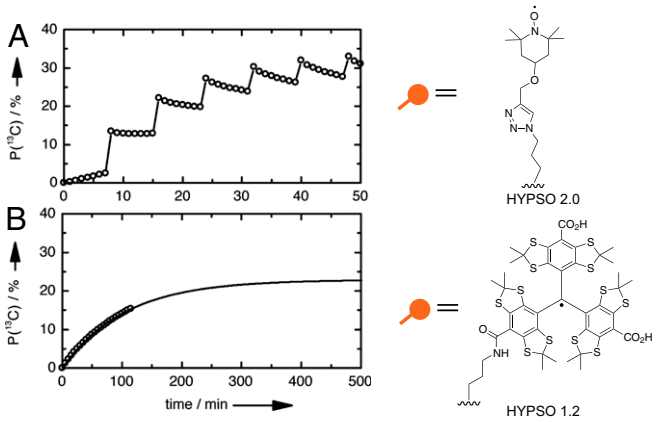

Fig. 3. (*A*) $^{1}H \rightarrow ^{13}C$ CP-DNP performed on 20 mg HYPSO 2.0 material (41 μmol/g) impregnated with 36 μL 3 M solution of [1-^{13}C]-pyruvate in D_2O. $P(^{13}C) > 30\%$ is reached in 32.5 min with $^{1}H \rightarrow ^{13}C$ CP applied at 7.5-min intervals. (*B*) Direct ^{13}C DNP performed on 20 mg HYPSO 1.2 material (16 μmol/g) impregnated with 36 μL 3 M solution of [1-^{13}C]-pyruvate in D_2O. $P(^{13}C) = 15\%$ is achieved after 2 h with a monoexponential buildup time $\tau_{DNP}(^{13}C) = 104.6 \pm 2.4$ min, potentially toward a maximum $P(^{13}C)^{max} = 22.9\%$. Note that the horizontal scale has been extended by a factor of 10 for *B* with respect to *A*. Schematic representations of the radicals in the materials are given in *A*, *Right* and *B*, *Right*.

approach. The corresponding grafted materials at similar concentrations gave poor polarization ($\varepsilon_{DNP} = 2$), because they do not meet the requirement of a homogeneous distribution of radicals. The fact that the solution is radical-free is illustrated by the fact that the measured ^{13}C T_1 is found to be ~50 s.

Fig. 2 allows one to compare the hyperpolarized [1-^{13}C]-pyruvate and [1-^{13}C]-acetate signals after dissolution with respect to their thermal equilibrium values, confirming nuclear spin polarizations as high as $P(^{13}C) = 25.3\%$ and $P(^{13}C) = 16.5\%$, respectively. As proof of general applicability, the same experiment was also performed on fumarate [with $P(^{13}C) = 19.9\%$ for both carbonyl carbons] and the dipeptide alanine-glycine [with $P(^{13}C) = 15.0\%$ and $P(^{13}C) = 13.6\%$ for the carbonyl carbons of alanine and glycine, respectively]. Note that the production of hyperpolarized solutions of folded proteins is still a challenge, mainly because of the rapid nuclear spin lattice relaxation rates at low magnetic field (leading to most of the hyperpolarization being lost during the dissolution process).

To optimize the materials, using optimal microwave frequency and power conditions ($f_{\mu w} = 188.3$ GHz and $P_{\mu w} = 100$ mW), we investigated the influence of the PA density in HYPSO 1.0 on polarization efficiency. The proton polarization displays a broad optimum around 88 μmol·g^{-1} (Fig. S1*A*), which roughly corresponds to an electron concentration of 49 mM in the pores, close to the optimal value of 50 mM that is normally used in D_2O:glycerol-d_8 mixtures (12). Note that the DNP enhancement measured as a function of the applied microwave frequency depicts a curve (often called microwave spectrum) that is similar to that typically obtained for DNP in frozen glasses without porous materials: two DNP optima are reached for positive or negative polarization at microwave frequencies $f_{\mu w} = 187.85$ and 188.3 GHz, respectively (Fig. S1*B*). The DNP obtained as a function of microwave power (often called a saturation curve) at $T = 1.2$ K indicates that 80% of the full saturation can be attained with a moderate power of $P_{\mu w} = 100$ mW (Fig. S1*C*). Although all of these parameters were carefully optimized, the polarization $P(^{13}C) = 25.3\%$ in [1-^{13}C]-pyruvate obtained with HYPSO 1.0 is somewhat lower than the record $P(^{13}C) = 40\%$ previously reported (12).

$P(^{13}C)$ can be increased to 36% in [1-^{13}C]-pyruvate (Fig. 3*A*) (39) on additional tuning of the PA through the incorporation of the TEMPO functionalities in HYPSO 2.0 (shown schematically in Fig. 3*A*) using a different linker and Click chemistry, which increases the yield of incorporation (details in *SI Methods*, Fig. S2, and Tables S1 and S2) (40).

Another important asset of HYPSO materials is that glassing agents, such as glycerol or DMSO, which may be proscribed in certain applications (e.g., in vivo imaging as well as the monitoring of chemical/enzymatic reactions, where the glassing agent may not be innocuous), are not required, because the matrix itself prevents crystallization. A clear demonstration of this feature is given with the example of the polarization of pure H_2O:D_2O [10:90 (vol:vol)] (Fig. S3).

Furthermore, these platform materials allow access to a broad range of solid polarizing matrices (for instance, with silica materials containing trityl radical functionalities). For example, direct ^{13}C polarization with trityl radicals might be preferred over indirect $^{1}H \rightarrow ^{13}C$ CP DNP with TEMPO (because the recently introduced $^{1}H \rightarrow ^{13}C$ CP technology is not yet commercially available). Preliminary results with a first generation of HYPSO 1.2 materials (Fig. 3*B*, *SI Methods*, Fig. S2, and Tables S1 and S2) with 16 μmol trityl functionalities per gram yield 15% ^{13}C polarization after 2 h, with potential for 25% at saturation (Fig. 3*B*).

In conclusion, D-DNP can be performed very efficiently using the HYPSO family of PAs. The sample preparation is carried out without glassing agents to provide pure hyperpolarized solutions (no radical contamination), which can easily be separated from the polarizing solids using standard filters. The efficiency of these solid polarization matrices is the result of the controlled incorporation of a homogeneous distribution of radicals along the pore channels of a highly porous mesostructured material. Although already shown here with pyruvate, acetate, fumarate, pure water, and a dipeptide (alanine-glycine), the approach should be applicable to a broad range of molecules that can be hyperpolarized by D-DNP (41).

Methods

Low-Temperature DNP with $^{1}H \rightarrow ^{13}C$ CP. The DNP apparatus is equipped with a DNP insert that comprises a microwave shield coupled to an oversized circular waveguide for microwave irradiation and a doubly resonant NMR Helmholtz coil of 0.5 cm^3 inner volume (^{13}C and ^{1}H at 71.73 and 285.23 MHz, respectively). The main axis of the radiofrequency (rf) coil is parallel to the static field to enable rapid dissolution. An ELVA (VCOM 10/94/400) microwave source operating at $f_{\mu w} = 94$ GHz ± 250 MHz up to $P_{\mu w} = 400$ mW is coupled to a VDI doubler (D200) with ~30% power conversion efficiency. The ^{1}H spins are polarized by microwave irradiation ($f_{\mu w} = 188.3$ GHz and $P_{\mu w} = 100$ mW) at $T = 1.2$ K. The proton polarization $P(^{1}H)$ is boosted by DNP and subsequently transferred by CP from ^{1}H to ^{13}C. The ^{13}C polarization builds up an iterative CP scheme, comprising two pairs of chirp pulses applied to both ^{1}H and ^{13}C channels with 1-ms duration, 100-kHz sweep width, and $B_1 = 30$ kHz rf amplitude. The ^{13}C polarization is monitored by application of 5° nutation pulses every 30 s. Because the rf fields are currently not sufficiently intense to compete with the dipolar interactions among the protons, the CP transfer is not 100% efficient, and therefore, only a fraction of $P(^{1}H)$ is transferred to ^{13}C. To further enhance $P(^{13}C)$, we reiterate the CP step $5 < n < 20$ times at intervals of 180 s.

Dissolution Experiments. Dissolution is performed with 5 mL superheated D_2O ($T = 450$ K and $P = 1$ MPa). The time sequence for the whole experiment is as follows: dissolution in $t_{diss} = 700$ ms, transfer in $t_{transfer} = 5$ s, injection in $t_{inject} = 3.5$ s, and settling in the NMR tube during $t_{settle} = 1$ s. Overall, the liquid-state NMR experiment can start 10.2 s after dissolution.

Liquid-State NMR Experiments. After DNP and dissolution, a series of ^{13}C NMR spectra of [1-^{13}C]-pyruvate is measured in a 7-T NMR spectrometer (300 MHz for protons) every 5 s with 5° pulses. After the hyperpolarization has completely relaxed to Boltzmann equilibrium, a thermal equilibrium spectrum is measured for comparison with a train of 90° nutation angle pulses (for example, 128 scans) and a long recycle delay (here, 350 s) to allow full relaxation.

ACKNOWLEDGMENTS. The authors thank Martial Rey and Dr. Pascal Miéville for valuable assistance. Transmission EM pictures were recorded by Dr. Frank Krumeich at the ScopeM. This work was supported by the Swiss National Science Foundation (SNF), the Ecole Polytechnique Fédérale de Lausanne, Eidgenössiche Technische Hochschule, the Swiss Commission for Technology and Innovation, Bruker BioSpin Switzerland AG, the Centre National de la Recherche Scientifique, Lyon Science Transfert Grant LST-1065, Equipements d'Excellence (EQUIPEX) Contract ANR-10-EQPX-47-01, European Research Council (ERC) Advanced Grants 320860 and 339754, and SNF grants.

1. Abragam A, Goldman M (1978) Principles of dynamic nuclear-polarization. *Rep Prog Phys* 41(3):395–467.
2. Ardenkjaer-Larsen JH, et al. (2003) Increase in signal-to-noise ratio of > 10,000 times in liquid-state NMR. *Proc Natl Acad Sci USA* 100(18):10158–10163.
3. Bowen S, Sekar G, Hilty C (2011) Rapid determination of biosynthetic pathways using fractional isotope enrichment and high-resolution dynamic nuclear polarization enhanced NMR. *NMR Biomed* 24(8):1016–1022.
4. Hilty C, Bowen S (2010) Applications of dynamic nuclear polarization to the study of reactions and reagents in organic and biomolecular chemistry. *Org Biomol Chem* 8(15):3361–3365.
5. Lee Y, Heo GS, Zeng H, Wooley KL, Hilty C (2013) Detection of living anionic species in polymerization reactions using hyperpolarized NMR. *J Am Chem Soc* 135(12): 4636–4639.
6. Chen HY, Ragavan M, Hilty C (2013) Protein folding studied by dissolution dynamic nuclear polarization. *Angew Chem Int Ed Engl* 52(35):9192–9195.
7. Nelson SJ, et al. (2013) Metabolic imaging of patients with prostate cancer using hyperpolarized [1-C-13]pyruvate. *Sci Transl Med* 5(198):198ra108.
8. Hartmann SR, Hahn EL (1962) Nuclear double resonance in the rotating frame. *Phys Rev* 128(5):2042–2053.
9. Jannin S, Bornet A, Colombo S, Bodenhausen G (2011) Low-temperature cross polarization in view of enhancing dissolution dynamic nuclear polarization in NMR. *Chem Phys Lett* 517(4-6):234–236.
10. Bornet A, Melzi R, Jannin S, Bodenhausen G (2012) Cross polarization for dissolution dynamic nuclear polarization experiments at readily accessible temperatures 1.2 < T < 4.2 K. *Appl Magn Reson* 43(1-2):107–117.
11. Jannin S, Bornet A, Melzi R, Bodenhausen G (2012) High field dynamic nuclear polarization at 6.7 T: Carbon-13 polarization above 70% within 20 min. *Chem Phys Lett* 549:99–102.
12. Bornet A, et al. (2013) Boosting dissolution dynamic nuclear polarization by cross polarization. *J Phys Chem Lett* 4(1):111–114.
13. Batel M, et al. (2012) Dissolution dynamic nuclear polarization efficiency enhanced by Hartmann-Hahn cross polarization. *Chem Phys Lett* 554:72–76.
14. Miéville P, et al. (2010) Scavenging free radicals to preserve enhancement and extend relaxation times in NMR using dynamic nuclear polarization. *Angew Chem Int Ed Engl* 49(35):6182–6185.
15. Harris T, Bretschneider C, Frydman L (2011) Dissolution DNP NMR with solvent mixtures: Substrate concentration and radical extraction. *J Magn Reson* 211(1):96–100.
16. Ardenkjaer-Larsen JH, et al. (2011) Dynamic nuclear polarization polarizer for sterile use intent. *NMR Biomed* 24(8):927–932.
17. Leach AM, Miller P, Telfeyan E, Whitt DB; General Electric Co. (2009) Method and apparatus for the dissolution and filtration of a hyperpolarized agent with a neutral dissolution media. US Patent US2009263325-A1.
18. Lumata L, et al. (2011) BDPA: An efficient polarizing agent for fast dissolution dynamic nuclear polarization NMR spectroscopy. *Chemistry* 17(39):10825–10827.
19. Lumata L, et al. (2012) The efficiency of DPPH as a polarising agent for DNP-NMR spectroscopy. *RSC Adv* 2(33):12812–12817.
20. Song C, Hu KN, Joo CG, Swager TM, Griffin RG (2006) TOTAPOL: A biradical polarizing agent for dynamic nuclear polarization experiments in aqueous media. *J Am Chem Soc* 128(35):11385–11390.
21. Hu KN, Song C, Yu HH, Swager TM, Griffin RG (2008) High-frequency dynamic nuclear polarization using biradicals: A multifrequency EPR lineshape analysis. *J Chem Phys* 128(5):052302.
22. Dane EL, et al. (2012) Rigid orthogonal bis-TEMPO biradicals with improved solubility for dynamic nuclear polarization. *J Org Chem* 77(4):1789–1797.
23. Zagdoun A, et al. (2012) A slowly relaxing rigid biradical for efficient dynamic nuclear polarization surface-enhanced NMR spectroscopy: Expeditious characterization of functional group manipulation in hybrid materials. *J Am Chem Soc* 134(4):2284–2291.
24. Kiesewetter MK, Corzilius B, Smith AA, Griffin RG, Swager TM (2012) Dynamic nuclear polarization with a water-soluble rigid biradical. *J Am Chem Soc* 134(10):4537–4540.
25. Zagdoun A, et al. (2013) Large molecular weight nitroxide biradicals providing efficient dynamic nuclear polarization at temperatures up to 200 K. *J Am Chem Soc* 135(34):12790–12797.
26. Sauvée C, et al. (2013) Highly efficient, water-soluble polarizing agents for dynamic nuclear polarization at high frequency. *Angew Chem Int Ed Engl* 52(41):10858–10861.
27. Lee Y, Zeng H, Ruedisser S, Gossert AD, Hilty C (2012) Nuclear magnetic resonance of hyperpolarized fluorine for characterization of protein-ligand interactions. *J Am Chem Soc* 134(42):17448–17451.
28. Lee Y, et al. (2012) Hyperpolarized binding pocket nuclear Overhauser effect for determination of competitive ligand binding. *Angew Chem Int Ed Engl* 51(21): 5179–5182.
29. Eichhorn TR, et al. (2013) Hyperpolarization without persistent radicals for in vivo real-time metabolic imaging. *Proc Natl Acad Sci USA* 110(45):18064–18069.
30. Gitti R, et al. (1988) Solid liquid intermolecular transfer of dynamic nuclear-polarization-enhanced flowing fluid h-1-nmr signals via immobilized spin labels. *J Am Chem Soc* 110(7):2294–2296.
31. Dollmann BC, et al. (2010) Thermoresponsive, spin-labeled hydrogels as separable DNP polarizing agents. *Phys Chem Phys* 12(22):5879–5882.
32. McCarney ER, Han S (2008) Spin-labeled gel for the production of radical-free dynamic nuclear polarization enhanced molecules for NMR spectroscopy and imaging. *J Magn Reson* 190(2):307–315.
33. Cassidy MC, Ramanathan C, Cory DG, Ager JW, Marcus CM (2013) Radical-free dynamic nuclear polarization using electronic defects in silicon. *Phys Rev B* 87(16): 161306.
34. Gajan D, et al. (2013) Solid-phase polarization matrixes for dynamic nuclear polarization from homogeneously distributed radicals in mesostructured hybrid silica materials. *J Am Chem Soc* 135(41):15459–15466.
35. Conley MP, Copéret C, Thieuleux C (2014) Mesostructured hybrid organic-silica materials: Ideal supports for well-defined heterogeneous organometallic catalysts. *ACS Catal* 4(5):1458–1469.
36. Comment A, et al. (2007) Design and performance of a DNP prepolarizer coupled to a rodent MRI scanner. *Concepts Magn Reso B* 31B(4):255–269.
37. Comment A, et al. (2008) Principles of operation of a DNP prepolarizer coupled to a rodent MRI scanner. *Appl Magn Reson* 34(3-4):313–319.
38. Jannin S, et al. (2008) A 140 GHz prepolarizer for dissolution dynamic nuclear polarization. *J Chem Phys* 128(24):241102.
39. Bornet A, et al. (2014) Microwave frequency modulation to enhance dissolution dynamic nuclear polarization. *Chem Phys Lett* 602:63–67.
40. Kolb HC, Finn MG, Sharpless KB (2001) Click chemistry: Diverse chemical function from a few good reactions. *Angew Chem Int Ed Engl* 40(11):2004–2021.
41. Vuichoud B, et al. (2014) Hyperpolarization of deuterated metabolites via remote cross-polarization and dissolution dynamic nuclear polarization. *J Phys Chem B* 118(5): 1411–1415.

Supporting Information

Gajan et al. 10.1073/pnas.1407730111

SI Methods

Materials Synthesis: Hybrid Polarizing Solids 1.0, 2.0, and 1.2.

1) Synthesis of hybrid polarizing solid 1.0. $MatPrN_3$ 1/X, $MatPrNH_2$ 1/X, and MatTEMPO 1/X [renamed hybrid polarizing solid 1.0 (HYPSO 1.0)] were prepared according to the literature (1).

2) Synthesis of HYPSO 2.0.

O-propargyl 2,2,6,6-tetramethyl-piperidine-1-oxyl. Under an argon atmosphere, NaH (2.72 g, 67.9 mmol) was added to dry *N,N*-dimethylformamide (DMF) (300 mL) and cooled to 0 °C (2). To this suspension, 2,2,6,6-tetramethyl-piperidine-1-oxyl (TEMPO; 9.00 g, 52.2 mmol) was added in portions. The reaction mixture was stirred for 30 min at 25 °C and then, cooled again to 0 °C before propargyl bromide (80% wt in toluene, 10.1 g, 67.9 mmol) was added dropwise. The resulting reaction mixture was then stirred for 3 h at 25 °C. Then, H_2O (300 mL) was added, and the product was extracted with EtOAc (3 × 150 mL). The combined organic layers were dried with brine and Na_2SO_4 and fully concentrated in vacuo. Column chromatography [heptane → 10% (vol/vol) EtOAc in heptane] yielded O-propargyl TEMPO (6.93 g, 63%) as an orange solid.

HYPSO 2.0. Under an argon atmosphere, O-propargyl TEMPO (369 mg, 1.75 mmol) was added to a suspension of $MatPrN_3$ 1/140 (3.00 g, 0.351 mmol azide) in DMF (40 mL) and Et_3N (1.5 mL). Then, a solution of CuI (3.3 mg, 18 μmol) in DMF/Et_3N (1:1; 500 μL) was added. The mixture was stirred for 48 h at 50 °C, filtrated, and washed with DMF (2 × 20 mL), EtOH (3 × 20 mL), and Et_2O (2 × 20 mL). The product was dried under vacuum (10^{-5} mbar) at 100 °C for 15 h.

3) Preparation of HYPSO 1.2.

Trityl alcohol. Tritert-butyl 8,8',8''-(hydroxymethanetriyl)Tris (2,2,6,6-tetramethylbenzo[1,2-d:4,5-d']bis([1,3]dithiole)-4-carboxylate) was prepared according to the literature (3).

HYPSO 1.2. Trityl alcohol (226 mg, 0.190 mmol) was dissolved in trifluoroacetic acid (TFA) (12 mL) and stirred under an argon atmosphere for 24 h. Then, the TFA was carefully evaporated in vacuo and replaced by dry dichloromethane (DCM) (5 mL). Oxalyl chloride (316 mg, 2.49 mmol) was dropwise added, and finally, two drops of dry DMF were added. The mixture was stirred for 4 h, during which time the color changed from yellow/dark brown to dark red. The solvent was evaporated until dryness, and the resulting red solid was redissolved in dry DCM (5 mL). To this solution, *N,N*-diisopropylethylamine (DIPEA) (33 μL, 0.19 mmol), 4-dimethylaminopyridine (DMAP) (2 mg, 20 μmol), and $MatPrNH_2$ 1/55 (500 mg, 0.146 mmol) were added. The mixture was stirred vigorously for 48 h, after which H_2O (1 mL) and DIPEA (60 μL, 0.38 mmol) were added. The mixture was stirred for 1 h to hydrolyze the unreacted acyl chlorides moieties (color changed from red to green), and then, it was filtrated, washed with DCM (3 × 5 mL) and Et_2O (3 × 5 mL), and dried under high vacuum (10^{-5} mbar) at 135 °C for 15 h (Tables S1 and S2).

Sample Preparation for Dissolution Dynamic Nuclear Polarization. Three different solutions were prepared.

i) Sodium [1-^{13}C]-pyruvate (3 M) in D_2O/H_2O [90%/10% (vol/vol)] with an NaH_2PO_4/Na_2HPO_4 buffer at pH 7.5–8.

ii) Sodium [1-^{13}C]-acetate (3 M) in D_2O/H_2O [90%/10% (vol/vol)].

iii) A mixture of sodium fumarate/alanine-glycine [$CH_3CH(NH_2)^{13}CONHCH_2{}^{13}COOH$]/sodium [1-^{13}C]-acetate (1 M/1 M-1 M) in D_2O/H_2O [90%/10% (vol/vol)].

Typically, 20 mg HYPSO materials are impregnated with 36 μL solution [*V* (microliters) = 1.8 m (milligrams)], and the wetted solid is placed in the home-built prepolarizer.

1. Gajan D, et al. (2013) Solid-phase polarization matrixes for dynamic nuclear polarization from homogeneously distributed radicals in mesostructured hybrid silica materials. *J Am Chem Soc* 135(41):15459–15466.
2. Gheorghe A, Matsuno A, Reiser O (2006) Expedient immobilization of TEMPO by copper-catalyzed azide-alkyne [3+2]-cycloaddition onto polystyrene resin. *Adv Synth Catal* 348(9): 1016–1020.
3. Reddy TJ, Iwama T, Halpern HJ, Rawal VH (2002) General synthesis of persistent trityl radicals for EPR imaging of biological systems. *J Org Chem* 67(14):4635–4639.

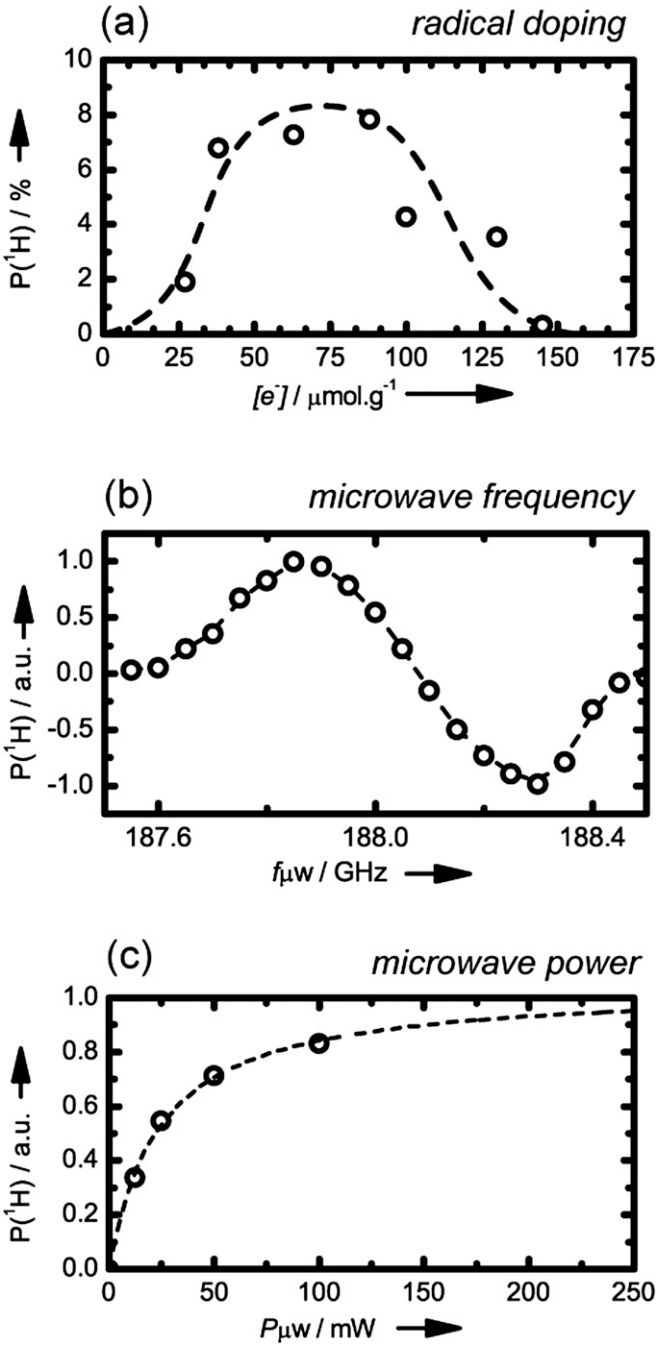

Fig. S1. (*A*) Optimization of the polarizing agent concentration in HYPSO 1.0. Maximum ^{1}H polarization was obtained in 40 μL H_2O/D_2O [10:90 (vol:vol)] mixtures in 20 mg different samples at $T = 4.2$ K and $B_0 = 6.7$ T. The optimization was performed at $T = 4.2$ K rather than $T = 1.2$ K, because the buildup times are faster. The electron concentration in the materials ranges from 25 to 140 μmol·g^{-1}. The polarization achieved with HYPSO 1.0 containing 88 μmol·g^{-1} TEMPO functionalities depends on the microwave power and microwave frequency. (*B*) The dynamic nuclear polarization (DNP) as a function of microwave frequency measured at $T = 4.2$ K displays a shape similar to that typically obtained for DNP in frozen glasses without porous materials. Positive and negative extrema occur for $f_{\mu w}^{+} = 187.85$ and 188.3 GHz, respectively. (*C*) The DNP microwave saturation curve measured at $T = 1.2$ K indicates that only 100 mW suffice to achieve at least 80% of full saturation.

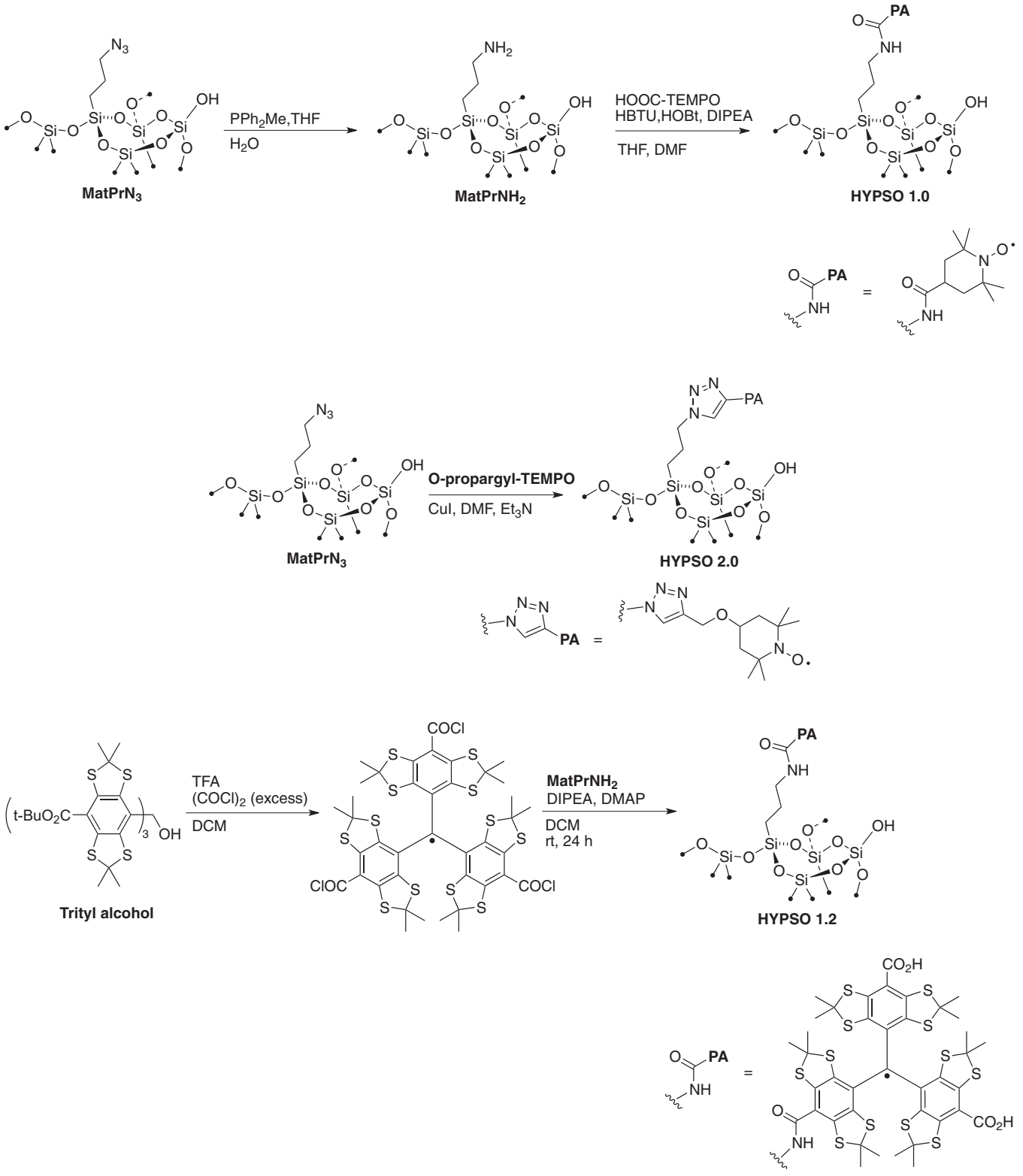

Fig. S2. Synthesis steps for the preparation of HYPSO 1.0, 2.0, and 1.2. THF, tetrahydrofuran.

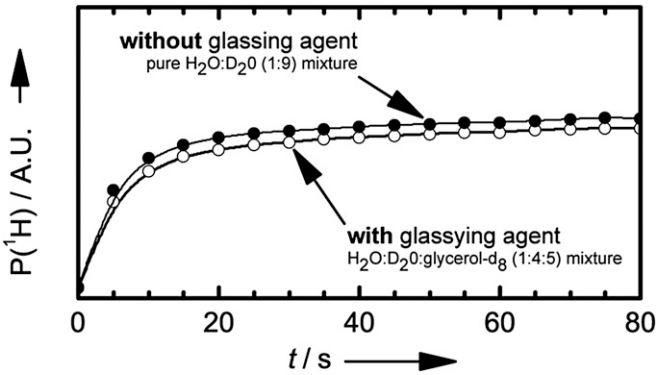

Fig. S3. Comparison between the ^{1}H dynamic nuclear polarization buildup at $T = 4.2$ K in 40 μL H_2O:D_2O mixture [10:90 (vol:vol); ●] and H_2O:D_2O:glycerol-d_8 mixture [10:40:50 (vol:vol:vol); ○] impregnated into 20 mg 88 μmol·g^{-1} HYPSO 1.0 at $T = 4.2$ K. Not only does the presence of the glass-forming agent glycerol not improve the efficiency of dynamic nuclear polarization, but it has a slightly deleterious effect.

Table S1. N_2 adsorption at 77 K and X-ray diffraction analysis

	N_2 adsorption/desorption*			X-ray diffraction			
Material	d_p (nm)†	a_s ($m^2 \cdot g^{-1}$)‡	V_p ($cm^3 \cdot g^{-1}$)§	Structure	d(100) (nm)	A_0 (nm)	Wall (nm)¶
HYPSO 1.2	10.6	647	1.17	Hexagonal	11.5	13.2	2.6
HYPSO 2.0	8.0	849	1.04	Hexagonal	10.5	12.1	4.1

*All materials displayed typical type IV isotherms.
†Mean pore diameter of mesopores calculated using Barrett–Joyner–Halenda analysis of the adsorption curve.
‡Surface area calculated using Brunauer–Emmet–Teller analysis.
§Pore volume calculated using Barrett–Joyner–Halenda analysis.
¶Wall thickness calculated by $A_0 - d_p$.

Table S2. EPR analysis

Material	Radical conc. (mmol g^{-1})	Line width (G)	Yield by EPR (%)
HYPSO 1.2	0.016	2.3	7
HYPSO 2.0	0.041	12.1	36